Performance Evaluation of a Full-Scale Deep U-Tube Utilizing Ozonated Oxygen as the Process Gas for Treating Drinking Water

K. Muroyama, E. Shibutani, T. Tsuji,* and M. Shimizu
Department of Chemical Engineering, Kansai University,
Osaka, 564-8680, Japan, e-mail:muroyama@ipcku.kansai-u.ac.jp
*JFE Engineering, Kawasaki City, Kanagawa, 210-0855, Japan

A deep U-tube for treating drinking water is composed of a coaxial inner tube serving as an efficient concurrent down-flow ozone dissolver and an outer column carrying out reactions between ozone and organic substances dissolved in the water after sedimentation treatment. In the present study, we developed a novel simulation model of the U-tube reactor, assuming that the U-tube is composed of a plug flow section (inner tube) followed by a tanks-in-series section (outer bubble column) and taking into account the reactions involved, and the effects of the hydrostatic pressurization on the flow and absorption equilibrium for the ozone and inactive gases in developing the mass balance models. We constructed an algorithm to evaluate the U-tube reactor performance based on the mass balance models. The hydrodynamics and mass transfer characteristics in the inner tube were measured and their correlations were incorporated in the simulation model. Available literature data and correlations on the rates of reactions between ozone and organic substances, the gas-liquid equilibrium for the active and inactive gases and the fluid mixing properties were also incorporated in the simulation model. The simulation results well explained the available data on the ozone absorption efficiency and the removal efficiency of odorous material (2-MIB) in a pilot plant and a real U-tube reactor. It is found that the ozone absorption is practically a single function of the gas/liquid ratio, while the decomposition efficiency of 2-MIB is a single function of the ozone dose for the water quantity to be treated.

Key words:
Drinking water, ozone, deep U-tube reactor, scale-up, ozone absorption, decomposition of 2-MIB

Introduction

Due to eutrophication the increased inclusion of nitric and phosphate compounds and humic substances occurs in the river water, inevitably resulting in an excess chlorination which in turn generates unwanted chlorine compounds with toxic and carcinogen nature, such as trihalomethanes in the treated water. In an advanced drinking water treatment, the employment of an ozone treatment followed by an activated carbon adsorption is becoming popular in Japan.[1] Ozone can decompose odorous materials such as geosmin and 2-methylisoborneol (2-MIB) and precursors to the trihalomethanes, thus reducing the occurrence of total chlorinated organic compounds. Note that ozone treatment is an environmental risk free process because the ozone readily self-decomposes into oxygen.[2] U-tube ozonation reactor is a novel bubble column constructed of a concentric downflow diffuser and an outer bubble column. In the downflow tube ozone-laden air or ozone-laden oxygen is mixed with river water treated with a sedimentation processing to achieve an efficient dissolution of

ozone under hydrostatic pressurization, while in the outer column the dissolved ozone reacts with the precursors to trihalomethanes and the odorous materials such as geosmin and 2-methylisoborneol (2-MIB) under a sufficient residence time to reduce the concentrations of these target materials within an allowable level. Hydrodynamics of the U-tube reactor was studied on the flow pattern and the gas holdup in the concurrent downflow tube was correlated by Roustan et al.[3–5] The liquid mixing properties in a full scale U-tube reactor were also studied by Roustan et al.[6]

In our previous study,[7] we proposed the design model of the U-tube ozonation reactor for treating drinking water, assuming that in the inner tube, the flows of gas and liquid are both in plug flow mode and in the outer tube, the flow of the gas is still in plug flow mode while the flow of the liquid can be modeled by tanks in series. The proposed simulation model well verified that the calculated results could well predict the data on the ozone absorption efficiency and the removal efficiency of odorous material (2-MIB).

In the preceding study,[8] we developed a novel design model for the U-tube reactor, in particular, considering the effect of hydrostatic pressurizations on the volumetric flow and the gas-liquid equilibriums for gaseous components including ozone and other inactive species and enabling a scale-up simulation from a pilot U-tube unit to a full-scale deep U-tube. The ozone absorption, the reaction between dissolved ozone and dissolved odorous material (2-MIB) in the liquid phase, the flow and mixing of both gas and liquid phases are combined to set up the multiple differential mass balance equations in the inner tube and the multiple mass balance difference equations based on the tanks-in-series model in the outer column. The physical absorption of inactive gases is also considered in the mass balance equations. An algorithm is constructed of the multiple mass balance equations with appropriate boundary conditions in the two reactor sections and solved to evaluate the reactor performance characteristics for a full-scale U-tube ozonation reactor treating drinking water. Available data on the reaction kinetics, gas-liquid equilibrium, mass transfer and fluid mixing reported in the literature or experimentally obtained by ourselves are also incorporated in the simulation calculations. Note that the data on the ozone absorption efficiency and the removal efficiency of the odorous material (2-MIB) were well predicted by the simulation calculation.

In the present study it is shown that the available data of reactor performance characteristics in a full-scale U-tube reactor are well predicted by the simulation calculations. It is also shown that the ozone absorption efficiency can be represented well by a single function of the gas/liquid ratio while the removal efficiency of 2-MIB can be represented by a single function of the ozone dose. The effects of column depth on the reactor performance characteristics are evaluated for the design of deep U-tube in a practical scale.

Experimental

Experimental apparatus

Fig. 1 shows the experimental U-tube apparatus for measuring the hydrodynamic properties and the gas-liquid mass transfer characteristics. The dimensions of the experimental column are as follows; the outer column is 454 mm in I.D. and 3550 mm in height, and the inner tube is 75 mm in I.D. and its end is opened at 100 mm above the outer column bottom. The inner tube is fitted coaxially in the outer column, and the length of its straight portion well exceeds the length of the outer column. The superficial velocities for the liquid and gas velocities in the inner tube were respectively ranged
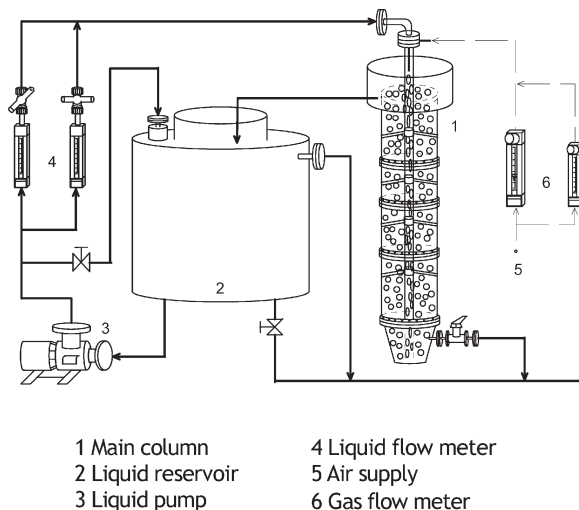

1 Main column   4 Liquid flow meter
2 Liquid reservoir   5 Air supply
3 Liquid pump   6 Gas flow meter

F i g . 1 – *Schematic diagram of experimental apparatus*

from 0.565 to 1. 885 m/s and from 0.0113 to 0.339 m/s. The gas distributor was a stainless steel pipe of 6 mm I.D. coaxially fitted at the top of the inner tube.

Gas holdup measurement

The axial distribution of gas holdup in the inner tube was measured using pairs of electro conductivity cells of thin 25×60 mm square stainless steel plates which were mounted facing each other on the opposite sides of the inner wall surface at 7 axial positions. After a steady state condition for the gas-liquid downflow was established in the inner tube, the inter-cell impedance was measured with 2 kHz AC by using a LCR meter (KC-547, KOKUYO Electric). In advance a correlation between the liquid holdup and the ratio of the inter-cell impedance for the single liquid flow to that for the gas-liquid flow or for the liquid-solid fluidization was obtained. Note that gas bubbles and glass beads are nonconductive and contribute the same role to the impedance at the same volumetric fraction in a conductive liquid. The gas holdup in the outer column was also measured using water manometer array based on a static pressure gradient method.

Volumetric mass transfer coefficient, $k_L a$, in the inner tube

Volumetric mass transfer coefficient in the inner tube was measured by physical absorption of pure oxygen; the pure oxygen gas was bubbled into the down-flowing water at a controlled rate through the single pipe distributor fitted at the top in the inner tube, while nitrogen gas was bubbled through a ring-shaped sparger fitted at the bottom in the outer column at a sufficiently high rate to desorp oxygen from the water. After a steady state was established,

the dissolved oxygen concentrations at the inlet and outlet of the inner tube were measured simultaneously with DO meters (YSI Model 58, YSI Japan). The axial differential mass balance equations are formulated to solve the oxygen concentrations in the liquid and gas phases based on the assumption that the gas and liquid flow downward in plug flow modes and the value of the volumetric mass transfer coefficient $k_L a$ is a constant along the entire inner tube length, while the effects of the hydrostatic pressure at any axial position on the volumetric gas flow rate and the gas-liquid equilibrium are considered. The multiple first order differential equations were numerically solved to determine an optimal value of $k_L a$ by an iterative procedure by fitting the calculated outlet dissolved oxygen concentration with the observed one. The mass balance equations and the iterative procedures to solve their equations are the same as those described for the absorption of inactive gases in the later section and omitted here.

Experimental results

Gas holdup in the inner tube

The gas holdup, ε_g, in the inner tube is plotted against the superficial gas velocity in Fig. 2. The value of ε_g in the concurrent downflow increases with increasing superficial gas velocity, while it significantly decreases with increasing liquid velocity. This may be explained as follows; in the high shear condition at a high downward liquid velocity the bubbles are finely divided and homogeneously dispersed in the continuous liquid. The increase of liquid flow rate steadily increases the downward velocity of the gas bubbles and then the gas holdup decreases with increasing liquid velocity.

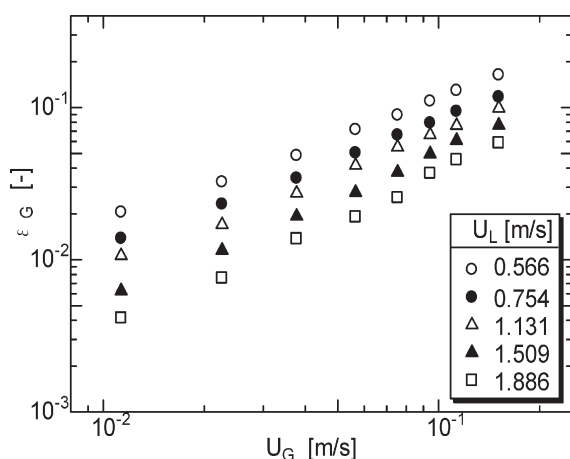The gas holdups in two-phase bubble flow systems with concurrent upflow and downflow were

well correlated by Clark and Flemmer[9] based on the drift flux model derived by Zuber and Findley[10] as follows:

$$\frac{U_G}{\varepsilon_G} = C_0(U_G + U_L) \pm 1.53\left(\frac{g\Delta\rho\sigma}{\rho_L^2}\right)^{1/4} \quad (1)$$

where C_0 depends on the flow direction of the two-phase flow and the gas holdup as given by,

$$C_0 = 0.934(1 + 1.42\varepsilon_G) \text{ (upflow)} \quad (2a)$$

$$C_0 = 1.52(1 - 3.67\varepsilon_G) \text{ (downflow)} \quad (2b)$$

Here the (+) sign and (–) sign in the second term in the r.h.s of Eq. (1) denotes upflow and downflow, respectively.

According to the drift flux model by Zuber and Findley, the following empirical equation is developed for the gas holdup in the present concurrent downflow system with the single pipe distributor by a regression analysis;

$$\frac{U_G}{\varepsilon_G} = 1.49(U_G + U_L) - 0.25. \quad (3)$$

Fig. 3 shows the plot of the term, U_G/ε_G, versus the term, $(U_G + U_L)$, for the gas holdup data in the inner tube of the U-tube column. The gas holdup data are correlated well by Eq. (3) with a coefficient of variation of 17.5 %. Note that the Clark and Flemmer correlation is located significantly below Eq. (3) indicating a large difference in the numerical constant to the term $(U_G + U_L)$ in both the downflow systems.
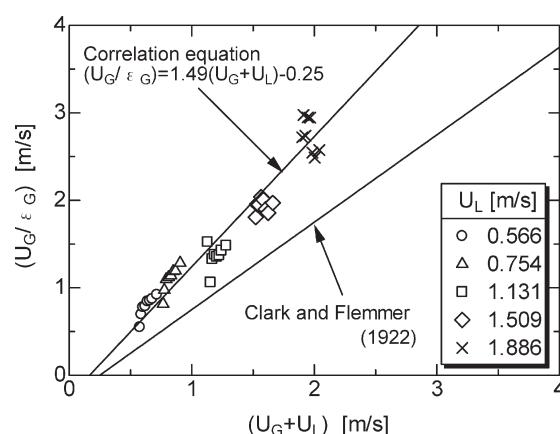

F i g . 3 – *Gas holdup correlation in the inner tube*

Gas-liquid volumetric mass transfer coefficient in the inner tube

Fig. 4 shows the plots of $k_L a$ values versus U_G in the inner tube for the single pipe gas distributor, indicating that the value of $k_L a$ increases with U_G.
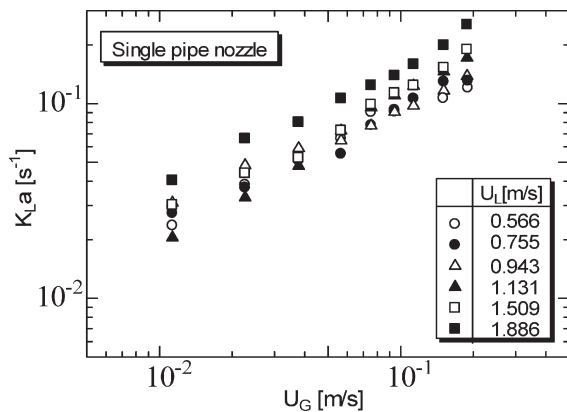

F i g . 2 – *Variation of ε_G versus U_G in the inner tube*

F i g . 4 – *Variation of $k_L a$ versus U_G in the inner tube*

Note that the values of $k_L a$ in the inner tube are significantly greater than those in a normal bubble column. The empirical correlations were formulated for the single pipe nozzles as follows;

$$k_L a = 0.452 U_L^{0.365} U_G^{0.628}. \tag{4}$$

Here the coefficient of variation between the predicted values of the volumetric coefficient by Eq. (4) and those of experimentally obtained is 13.3 %.

Modeling of U-tube reactor for simulation calculation

Model concept

In the inner tube of a deep U-tube reactor the gas and liquid flow concurrently downward in a dispersed gas bubble mode, at high velocities and with short residence times, for both the gas and liquid phases. In the outer column of the reactor the dispersed gas bubbles flow upward with a relatively short residence time, while the liquid flows slowly with a long residence time and suffers intense mixing as in a normal bubble column.

Considering the differences in the mixing behavior of liquid in the inner tube section and in the outer column section, we employed the plug flow model in the inner tube section and the series-in-tanks model in the outer column section, while the gas phase remains to be in a plug flow state in both sections. Mass balance modeling and necessary parameter setting in the two reactor sections will be described in the following for a particular U-tube operation using ozone-laden oxygen.

Mass balances in the inner tube section

Mass balance equations for the chemically active and inactive species are expressed by differen-

T a b l e 1 – *Mass balance equations in the inner tube section*

$$U_L \frac{dC_{LO_3}}{dz} = (k_L a)_{O_3}(C_{LO_3}^* - C_{LO_3}) - \tag{5}$$
$$-(1 - \varepsilon_G)(k_s C_{LO_3}^{1.5} + k_r C_{LO_3} X_s)$$

$$M_{O_3} \frac{dG_{O_3}}{dz} = -(k_L a)_{O_3}(C_{LO_3}^* - C_{LO_3}) \tag{6}$$

where $C_{LO_3}^*$ is defined as

$$C_{LO_3}^* = m_{O_3} C_{G_{O_3}} = G_{O_3} M_{O_3}/U_G \tag{7}$$

Mass balance equation for the liquid-phase inactive gas:

$$U_L \frac{dC_{Lj}}{dz} = (k_L a)_j(C_{Lj}^* - C_{Lj}) \tag{8}$$

Overall mass balance for j-th inactive gas:

$$G_j = G_{j0} - U_L(C_{Lj} - C_{Lj0})/M_j \tag{9}$$

where C_{Lj}^* is defined as

$$C_{Lj}^* = m_j C_{Gj}, \quad C_{Gj} G_j M_j/U_G \tag{10}$$

Total molar flow rate of gases, G_t:

$$G_t = G_{O_3} + \sum G_j \tag{11}$$

Mol fraction and partial pressure of a gas:

$$y_j = G_j/G_t, \quad p_j = P_t y_j \tag{12}$$

Static pressure:

$$P_t = P_0 + \rho_L(1 - \varepsilon_G)gz \tag{13}$$

Superficial gas velocity:

$$U_G = G_t RT/P_t \tag{14}$$

Boundary conditions for the gaseous species involved:

$$z = 0; \ G_{O_3} = G_{O_3 0}; \ C_{G_{O_3}} = C_{G_{O_3} 0}; \ G_j = G_{j0}; \ C_{Lj} = C_{Lj0} \tag{15}$$

Differential mass balance for ozone consuming substance and odorous material (2-MIB):

$$U_L \frac{dX_s}{dz} = -(1 - \varepsilon_G)k_d C_{LO_3} X_s \tag{16}$$

$$U_L \frac{dX_O}{dz} = -(1 - \varepsilon_G)k_O C_{LO_3} X_O \tag{17}$$

Boundary conditions for Eqs. (16) and (17):

$$z = 0; \quad X_s = X_{s0}; \quad X_O = X_{O0} \tag{18}$$

tial equations with their boundary conditions as given in Table 1. Note that the inactive gas indicated by j is oxygen in the present case. If ozonized air is used as the process gas, one more inactive gas, nitrogen, should be added.

Mass balances in the outer column

Mass balances for gas phase and liquid phase components in the i-th continuous tank are given in Table 2. The mass balance for the gas phase components are expressed by differential equations and those for the liquid phase components are expressed by difference equations.

T a b l e 2 – *Mass balance equations in the i-th vessel in the outer column*

Mass balance for the liquid phase ozone:

$$U_L(C_{LO_3,i} - C_{LO_3,i-1}) = M_{O_3}(G_{O_3,i-1} - G_{O_3,i}) - \qquad (19)$$
$$-(1-\varepsilon_G)L_i(k_sC_{LO_3,i}^{1.5} + k_rC_{LO_3,i}X_{S,i})$$

Differential mass balance for the gas phase ozone:

$$M_{O_3}\frac{dG_{O_3}}{dz} = -(k_La)_{O_3}(C_{LO_3}^* - C_{LO_3i}) \qquad (20)$$

where $C_{LO_3}^*$ is given by

$$C_{LO_3}^* = m_{O_3}C_{G_{O_3}}, \quad C_{G_{O_3}} = G_{O_3}M_{O_3}/U_G \qquad (21)$$

The boundary condition for Eq. (20):

$$z = 0; \quad G_{O_3} = G_{O_3,i-1} \qquad (22)$$

Differential mass balances for j-th inactive gas:

$$M_j\frac{dG_j}{dz} = -(k_La)_j(C_{Lj}^* - C_{Lj,i}) \qquad (23)$$

where C_{Lj}^* is given by the following relations,

$$C_{Lj}^* = m_jC_{Gj}; \quad C_{Gj} = G_jM_j/U_G \qquad (24)$$

Boundary condition for Eq. (23):

$$z = 0; \quad G_i = G_{j,i-1} \qquad (25)$$

Gas phase molar flow rate at the exit of i-th tank:

$$G_{j,i} = G_{j,i-1} - U_L(C_{Lj,i} - C_{Lj,i-1})/M_j \qquad (26)$$

The total molar flow rate of gases:

$$G_t = G_{O_3} + \sum G_j \qquad (27)$$

Mol fraction and partial pressure of a gas:

$$y_j = G_j/G_i, \quad p_j = P_t y_j \qquad (28)$$

Static pressure and superficial gas velocity:

$$P_t = P_0 + \rho_L(1-\varepsilon_G)gz \qquad (29)$$
$$U_G = G_tRT/P_t \qquad (30)$$

Mass balances for ozone consuming substance and odorous material (2-MIB):

$$U_L(X_{L,i-1} - X_{L,i}) = (1-\varepsilon_g)L_ik_dC_{LO}X_{S,i} \qquad (31)$$
$$U_L(X_{O,i-1} - X_{O,i}) = (1-\varepsilon_g)L_ik_oC_{LO}X_{O,i} \qquad (32)$$

Gas-liquid equilibrium and mass transfer characteristics

The dimensionless Henry's law constant, m_j [–] is defined as follows,

$$m_j = \frac{RT\rho_L}{H_j M_{H_2O}} \text{ [mol frac.]} \qquad (33)$$

where Henry's law constants for the inactive gases, H_j, were estimated from the correlations given in a handbook[11] and that for ozone-water system associated with self-decomposition of ozone was estimated from the correlation given by Miyahara et al.[12]

The volumetric mass transfer coefficients for the gaseous species except oxygen in the inner tube were estimated from the correlation obtained from the physical oxygen absorption, $(k_La)_{O_2}$, as follows,

$$\frac{(k_La)_j}{(k_La)_{O_2}} = \left(\frac{D_{Lj}}{D_{LO_2}}\right)^{0.5} \qquad (34)$$

where the diffusivities of the gaseous species were estimated from the Wilke-Chang correlation.[13]

The volumetric mass transfer coefficient in the outer column was estimated from the correlation by Akita and Yoshida[14] because the bubble flow mode and the gas holdup behavior in the outer column were the same to those in the normal bubble column because of low liquid velocity.

The gas holdup in the inner tube for the single pipe nozzle was calculated from the correlation obtained in the above section. The gas holdup in the outer column was estimated by the correlation presented by Akita and Yoshida.[14]

Mixing parameter in the outer tube

The number of series tanks indicating extent of liquid mixing in the outer tube section was evaluated as follows. The axial dispersion coefficient, D_z, in the normal bubble column can be estimated by the correlation of Deckwer[15] which covers a range of lower superficial gas velocities as exemplified in the outer column of the U-tube. The dimensionless standard deviation for the normalized residence time distribution for the axial dispersion model can be related to the inverse of the number of mixing tanks, J for the series in tanks model as follows;[16]

$$\frac{\sigma_P^2}{\bar{t}_P^2} = \left[\frac{2}{Pe} - \frac{2}{Pe}(1-\exp(-Pe))\right] = \frac{1}{J} \qquad (35)$$

where Pe is the Peclet number for the axial dispersion model, $Pe = U_LL/D_z$. From Eq. (35), a real

number, J, is obtained for a specific gas-liquid operating condition. In the simulation calculation of the series-in-tanks model, an additional reactor of a volume corresponding to the decimals part of J was connected to the last one of the equal-volume reactors corresponding to the integer part of J.

Kinetic parameters for the ozone oxidation reactions

The self decomposition rate can be approximated by the first to second order kinetics with respect to the dissolved ozone concentration in the pH-neutral water as encountered for the drinking water treatment.[12,17,18] It was found that the correlation equation for the kinetic constant proposed by Morioka et al.[18] deviates from other two correlations in the range of higher ozone concentration. Thus we employed the correlation of the kinetic constant for the ozone self-decomposition most recently presented by Miyahara et al.[12] whose correlation is shown bellow;

$$k_s = (4.0 \cdot 10^{11} + 9.6 \cdot 10^{14} [OH^-]^{0.8}) \cdot \\ \cdot \exp(-9.6 \cdot 10^3 / T) \quad (36)$$

Miyahara et al. also showed that the ozone decomposition rate is proportional to 1.5-th order of the dissolved ozone concentration.

Moniwa et al.[19] investigated the first order reaction rate constant for the ozone consumption rate constant and the decomposition rate constant for the reaction of ozone with dissolved organic materials as follows:

$$k_r = 0.6667 \ [m^3 \cdot kg^{-1} \cdot s^{-1}] \quad (37a)$$

$$k_d = 0.8333 \ [m^3 \cdot kg^{-1} \cdot s^{-1}] \quad (37b)$$

First order rate constant for the reaction of ozone with dissolved odorous material (2-MIB) was correlated by Morioka et al.[18] as follows:

$$k_o = \exp(45.0 + 0.9[pH]) \cdot \exp(-11100/T) \quad (38)$$

Note that Morioka et al.[20] investigated the kinetics of ozone decomposition of geosmin and 2-MIB under the presence of carbonate, free chlorine, alcohols and volatile fatty acids.

Operating conditions

Table 3 summarizes the major dimensions, and operating conditions for the pilot and full-scale U-tube reactors for which the axial distributions of the species involved, such as, liquid phase and gas phase ozone concentrations, and liquid phase concentration of odorous materials are numerically calculated, respectively in the inner tube and in the outer column. In the following the results for the

T a b l e 3 – *Dimensions and operating conditions for the pilot and the commercial U-tubes*

Operating condition	Unit	Pilot plant	Commercial plant
Column height	[m]	17.0	27.2
Inner tube diameter	[m]	0.047	0.77
Outer column diameter	[m]	0.312	3.95
Gas flow rate	[m³/s]	$1.04 \cdot 10^{-4}$	$1.89 \cdot 10^{-2}$
Liquid flow rate	[m³/s]	$5.36 \cdot 10^{-3}$	0.944
Influent ozone conc.	[kg/m³]	0.148	0.148
Gas/Liquid ratio	[–]	0.020	0.020
Ozone dose	[kg/m³]	0.00296	0.00296
Concentration of ozone consuming substances	[kg/m³]	$1.60 \cdot 10^{-3}$	$1.60 \cdot 10^{-3}$
Odorous material conc.	[kg/m³]	$1.107 \cdot 10^{-7}$	$1.107 \cdot 10^{-7}$
Gas velocity (inner tube)	[m/s]	$5.99 \cdot 10^{-2}$	$4.05 \cdot 10^{-2}$
Gas velocity (outer column)	[m/s]	$1.39 \cdot 10^{-3}$	$1.60 \cdot 10^{-3}$
Liquid velocity (inner tube)	[m/s]	3.09	2.03
Liquid velocity (outer column)	[m/s]	$7.17 \cdot 10^{-2}$	$8.01 \cdot 10^{-2}$
Residence time (inner tube)	[s]	5.5	13.4
Residence time (outer column)	[s]	237	340
Number of series-in-tanks	[–]	18.92	4.38
Water temp.	[°C]	20.0	20.0

full-scale U-tube reactor only are described; the results for the pilot plant and comparison between those for the pilot U-tube and for the full-scale U-tube reactors were described elsewhere.[8]

Algorithm and calculation procedure

In the inner tube section, the axially differential equations for the liquid-phase and gas-phase components including ozone, inactive gaseous components, and dissolved ozone consuming substances were solved by the Runge-Kutta-Gill method with the boundary conditions at the inlet of the inner tube. After determining the axial concentration distribution of these components, the liquid-phase concentration of odorous material was solved. The odorous material itself is included in the ozone consuming substances but the concentration of it is extremely less than that of the ozone consuming substances as shown in Table 3. Therefore the proce-

dure to solve the concentration of the odorous material is reasonable and does not cause any calculation errors in the concentrations of other species in the gas and liquid phases. In the column outer section, the difference mass balance equations for each mixed tank were solved by a trial-and-error procedure to fit the outlet liquid phase concentration with that from the overall mass balance between the phases. After determining the liquid phase concentrations, the concentration of odorous material was determined. The set of calculations were successively carried out from the initial to the final tank of the outer column. The algorithm was constructed based on the C++ language and all the calculations were carried out on a P.C.

Results of simulation and scale-up calculations

In the following, the simulation calculations are carried out for the U-tube reactor operated with ozonated oxygen since the full-scale plant operation for which we have successfully applied the simulation model in the present state[8] has been successfully demonstrated by using ozonated oxygen.

Axial distribution of related components

Fig. 5 shows the variations of the liquid phase and gas phase ozone concentrations versus axial depth in the inner tube and outer column sections in the commercial plant. Note that the equilibrium liquid-phase ozone concentration which is the product of dimensionless equilibrium constant and the gas phase ozone concentration, $m \cdot C_{GO_3}$, is shown in place of the real gas phase ozone concentration to indicate how the liquid phase ozone concentration closely approaches their equilibrium value with the gas phase ozone along the axial depth.
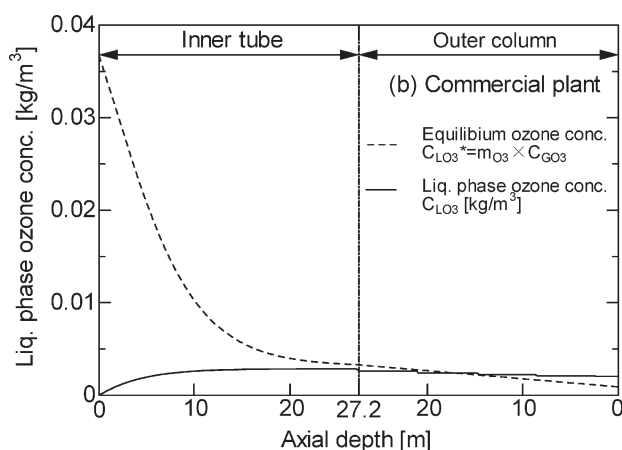
It is obvious that the dissolved ozone concentration increases with increasing axial depth in the inner tube while in the outer column it only slightly decreases with decreasing axial depth. It may be noted that in the full-scale plant the dissolved ozone concentration approaches the liquid-phase equilibrium ozone concentration at an axial depth of about 20 m, beyond which it becomes insensitive to the axial depth in the inner tube, while in the outer column it slightly decreases with decreasing axial depth, cross the liquid-phase equilibrium ozone concentration, and eventually lays below the latter in the upper half region of the outer column where the desorption of ozone from liquid to gas definitely occurs due to decreased hydrostatic pressure. The increase in the volumetric gas-liquid mass transfer, $k_L a$, could enhance the ozone dissolution within an initial 10 m axial depth from the top in the inner tube[8] but its extent was only slight. This is because in the deep full-scale reactor, the depth of the reactor is as high as 27.2 m and the increased hydrostatic head causes the enormous increase in the equilibrium ozone concentration with the gas phase concentration and makes the effect of $k_L a$ insensitive.

Fig. 6 shows the variation of liquid-phase odorous material concentration versus axial depth together with that of dissolved ozone consuming substances in the full-scale deep U-tube. In the full-scale reactor with a larger diameter of 3.95 m the number of the mixing tanks is only 4.4 and the concentration of the liquid-phase odorous material decreases in stepwise while the concentration drop in the first tank being the largest. Note that the concentration values at the position of exit of each tank may represent the real axial concentration distribution. Note that to improve the accuracy in the calculation model for the outer column the series tanks are considered to be composed of not only the number of tanks with an equal volume, corresponding to the integer part of the real number, J, derived from Eq. (35), but also an additional one of a smaller volume equivalent to the decimal fraction of J.
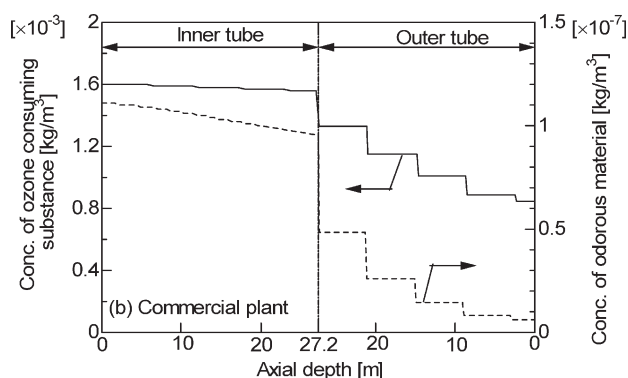

F i g . 5 – *Variations of liquid phase and gas phase ozone concentrations with axial depth*

F i g . 6 – *Variations of odorous material and ozone consuming substance with axial depth*

Axial distribution of inactive gas

In Fig. 7, axial distributions of gas-phase and liquid-phase concentrations of the inactive gas, oxygen, are shown for the specified conditions listed in Table 3 in the full-scale U-tube reactor. The gas-phase oxygen concentrations linearly increase with axial depth in the inner tube, and inversely linearly decrease with axial rise in the outer column due to the hydrostatic effect. The value of the liquid phase oxygen concentration also linearly increase with increasing axial depth in the inner tube, while in the outer column, it remains almost constant and does not reach the saturated oxygen concentration even at the exit of the outer column.
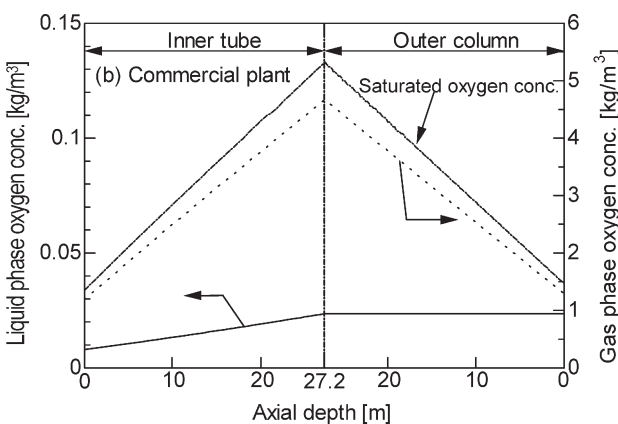
F i g . 7 – *Variations of oxygen concentrations with axial depth in the gas and liquid phases*

Fig. 8 shows the axial variations of the volumetric flow rate of gas, mainly consisted of oxygen, in the full-scale U-tube reactor for the $k_L a$ value estimated by Eq. (4). The volumetric gas flow rate decreases with axial depth, turns up at the column bottom and increases with decreasing axial depth in a concave shape. But it does not fully recover at the
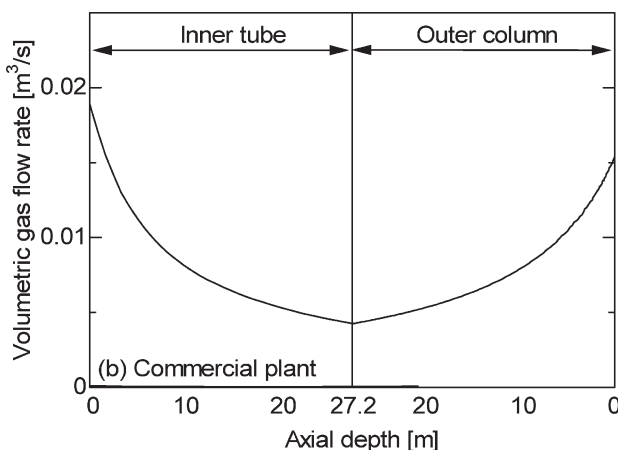
exit of the outer tube, indicating that the absorbed oxygen amount is 18.5 % of its supplied amount. This suggests that the recycle use of the remained oxygen, which is otherwise uselessly disposed, would improve the cost effectiveness and energy efficiency of the system, thus reducing the environmental impact.

Ozone absorption efficiency and removal efficiency of odorous material

Key factors indicating the reactor performances and operating conditions for ozonation treatment are defined as follows:

Ozone absorption efficiency (dimensionless) =

$$= \frac{(\text{Influent ozone conc.} - \text{Effluent ozone conc.})}{\text{Influent ozone conc.}}$$

Removal efficiency of odotous material (dimensionless) =

$$= \frac{(\text{Influent odotous material conc.} - \text{Effluent odorous material conc.})}{\text{Influent odorous material conc.}}$$

Ozone dose (kg · m^{-3}) = Influent ozone conc. · Gas/Liquid ratio

Gas/Liquid ratio (dimensionless) =

= Volumetric gas flow rate/Volumetric liquid flow rate

In order to verify the practical applicability of the scale-up simulation method developed in the present work, the measured data on the ozone absorption efficiency and the removal efficiency of odorous materials for a pilot and a full-scale U-tube reactors are compared with the calculated ones. Details of the calculation for the pilot scale U-tube unit were described in the preceding paper,[8] verifying that the ozone absorption efficiency and the removal efficiency of the odorous material were well predicted by the simulation model.

Figs. 9 and 10 show the measured values of ozone absorption efficiency with use of ozonated oxygen are compared with the calculated ones in the pilot and commercial plants, respectively. Note that the water temperature was considered to evaluate the mass transfer and equilibrium properties for the absorptions of gaseous components in the simulation calculation. It is apparent that in the pilot plant the ozone absorption efficiency could be well predicted by the simulation model indicated by the smaller CV values of 3.91 % and 1.24 %, respectively, for the ozonated air and for the ozonated oxygen as the process gases. Note that the values of ozone absorption efficiency for the ozonated oxygen are significantly greater than those for the ozonated air. Note also that the CV (coefficient of variation) value indicates the degree of relative deviation (normalized standard deviation) between the measured and calculated values of the ozone ab-
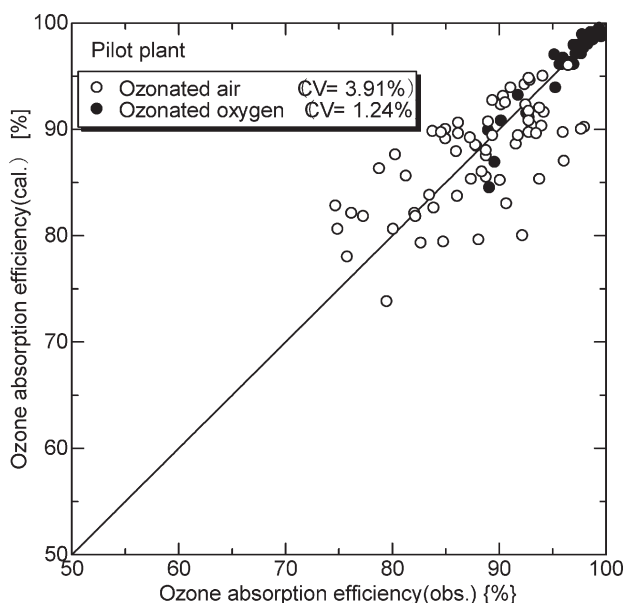

F i g . 8 – *Variation of volumetric gas flow rate with axial depth*

F i g . 9 – *Comparison between the ozone absorption effi-
ciency calculated with that observed in the pilot
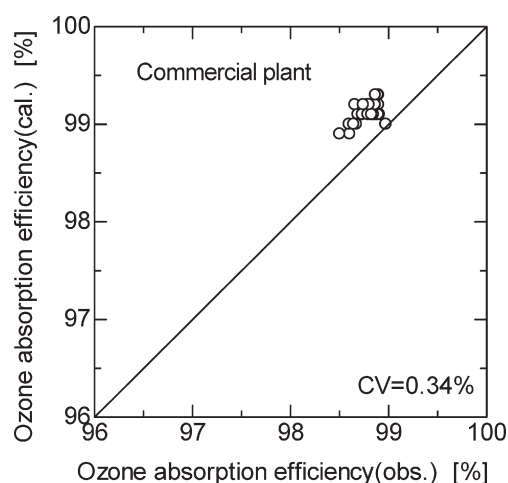plant*

F i g . 1 0 – *Comparison between the ozone absorption effi-
ciency calculated with that observed in the com-
mercial plant*

sorption efficiency. It is shown that the values of
the ozone absorption efficiency are high (about
99 %) and the CV value is only 0.34 % for the com-
mercial plant data using ozonated oxygen as the
process gas, showing that the prediction of ozone
absorption efficiency is excellent for the full-scale
deep U-tube.

Correlations of reactor performance indexes

Fig. 11 shows the effect of the gas/liquid ratio
on the ozone absorption efficiency in the full-scale
plant. The ozone absorption efficiency steadily de-
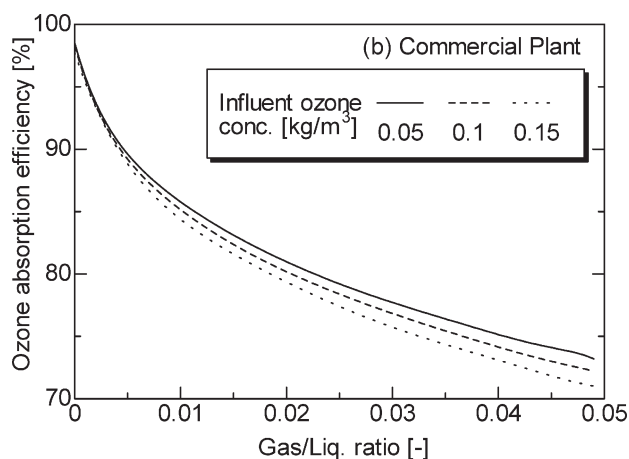creases with increasing gas/liquid ratio, while

F i g . 1 1 – *Effect of gas/liquid ratio on ozone absorption ef-
ficiency*

slightly decreases with increasing influent ozone
concentration. It is found that in the full-scale plant
with a depth of 27.2 m, the ozone absorption effi-
ciency is much higher than that in the pilot plant
with a depth of 17 m but the effect of the ozone
concentration on the ozone absorption is quite
small, as shown in Figs. 9 and 10. This may be due
to increased hydrostatic pressure, which linearly in-
creases the equilibrium liquid-phase ozone concen-
tration to the gas phase ozone and thus enhances the
mass transfer driving force. It may be pointed out
that the ozone absorption efficiency can be well
correlated by a single parameter of gas/liquid ratio
for the specified U-tube unit configuration.

Fig. 12 shows the diagrams indicating the ef-
fect of ozone dose on the removal efficiency of
odorous material (2-MIB) for the full-scale plant.
The removal efficiency steadily increases with in-
creasing ozone dose (loading), sharply in the range
of lower ozone dose and gradually approaches the
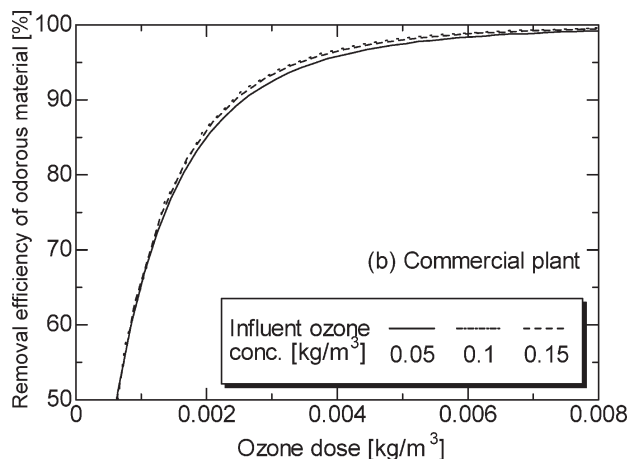line of 100 % in the range of higher ozone dose,

F i g . 1 2 – *Effect of ozone dose on removal efficiency of
odorous material*

while slightly increasing with increasing influent ozone concentration. It may be noted that the odorous material removal efficiency can be well correlated with a single parameter of ozone dose for the specified U-tube configuration.

Effect of axial depth on performance indexes of the U-tube

By varying the axial depth (column height) as 5, 10, 15, 20 and 27.2 m at a constant residence time of 340 s, together with the outer column diameter 9.21, 6.51, 5.32, 4.61 and 3.95 m, correspondingly, the simulation calculations were conducted for the U-tube reactors. In the calculation, the inner tube diameter was maintained at a common size of 0.770 m.

Fig. 13 shows the variation of ozone absorption efficiency versus axial depth at specified gas/liquid ratio values. It is apparent that the ozone absorption efficiency rapidly increases with increasing axial depth in the lower range of depth up to about 12 m, beyond which the increment of the ozone absorption efficiency against axial depth significantly decreases. In the higher range of axial depth above 20 m the ozone absorption efficiency only slightly increases with further increase of axial depth.
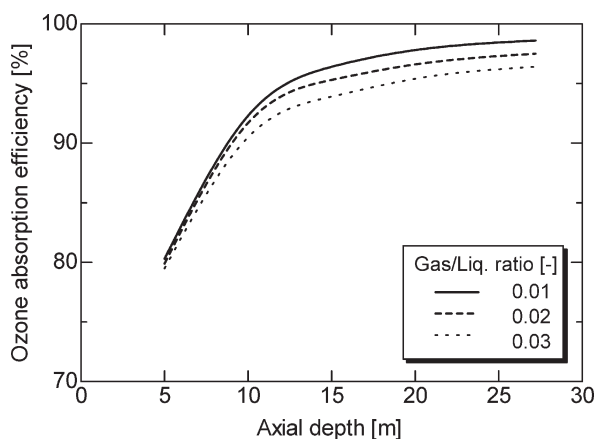

F i g . 1 3 – *Variation of ozone absorption efficiency*

Fig. 14 shows variation of the removal efficiency of odorous material versus axial depth at specified values of ozone dose in the range of 0.002-0.006 [kg/m³]. The removal efficiency of odorous material increases with increasing column depth, rather significantly at a small ozone dose value, 0.002 [kg/m³], but less significantly at larger ozone dose values. The axial height of the deep U-tube may be determined as a minimum height to establish the requirement of the allowable exit concentration level of the odorous material at available operating conditions for ozone dose and gas liquid ratio.
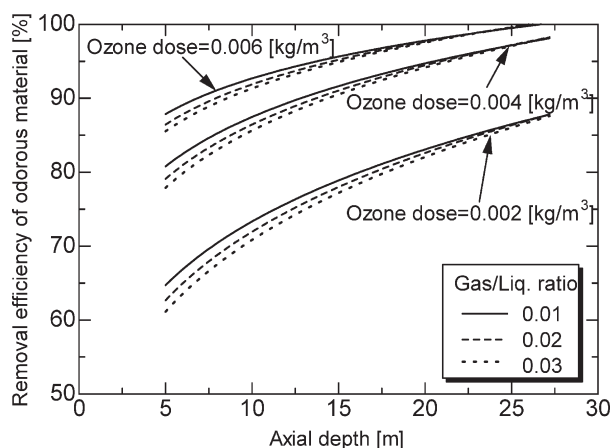

F i g . 1 4 – *Variation of removal efficiency of odorous material versus axial depth of the deep U-tube*

Conclusion

A novel simulation model was constructed of the U-tube ozonation reactor for treating drinking water under the assumption that in the inner tube, the flows of gas and liquid are both in plug flow modes, while in the outer tube, the gas phase flow is in the plug flow mode and the liquid phase flow is approximated by the tanks-in-series model. The effects of hydrostatic pressure on the gas-phase volumetric flow rate and on the gas-liquid equilibriums for ozone and other inactive components were taken into consideration at any axial position.

The ozone absorption, the reactions between dissolved ozone and dissolved organic species in the liquid phase, and the hydrodynamics and fluid mixing for the gas and liquid phases were combined to construct the multiple differential mass balance equations in the inner section, and multiple difference mass balance equations for each tank in the outer column section. Available data and correlations from the literatures on the reaction kinetics, gas-liquid equilibriums and hydrodynamic and mass transfer properties were incorporated. The unavailable data on the hydrodynamics and gas-liquid mass transfer properties were experimentally obtained and incorporated.

The simulation results well explained the available data of the ozone absorption efficiency and the removal efficiency of the odorous material in a pilot U-tube reactor utilizing the ozonated oxygen as the process gas for treating drinking water. The simulation procedure was also successfully extended to verify the performance of a full-scale U-tube reactor for ozone absorption efficiency.

It is shown that the ozone absorption efficiency can be correlated as a single function of the gas/liquid ratio and the removal efficiency of the odorous material can be correlated as a single function of the ozone

dose, respectively, in a practical level depending on the specified deep U-tube configuration.

It is indicated that that the ozone absorption efficiency rapidly increases with increasing axial depth in a lower range of depth up to about 12 m, beyond which the increment of the ozone absorption efficiency against axial depth significantly decreases. In the higher range of axial depth above 20 m the ozone absorption efficiency only slightly increases with further increase of axial depth.

ACKNOWLEDGEMENT

Notations

C_G – gas phase concentration, $kg \cdot m^{-3}$

C_L – liquid phase concentration, $kg \cdot m^{-3}$

C_L^* – equilibrium concentration, $kg \cdot m^{-3}$

D – diameter, m

D_L – molecular diffusivity, $m^2 \cdot s^{-1}$

D_z – axial dispersion coefficient, $m^2 \cdot s^{-1}$

d_{vs} – sauter diameter, m

E_L – energy dissipation rate per unit mass of liquid, $m^2 \cdot s^{-3}$

g – gravitational acceleration, $m \cdot s^{-2}$

G – molar flow rate, $mol \cdot m^{-2} \cdot s^{-1}$

H – Henry's law constant, $Pa \cdot mol\ frac.^{-1}$

J – number of mixing tanks, –

$k_L a$ – volumetric mass transfer coefficient, s^{-1}

k_d – decomposition rate const. for ozone consumption substances, $m^3 \cdot kg^{-1} \cdot s^{-1}$

k_o – decomposition rate const. for 2-MIB, $m^3 \cdot kg^{-1} \cdot s^{-1}$

k_r – decomposition rate const for dissolved organic substances, $m^3 \cdot kg^{-1} \cdot s^{-1}$

k_s – self-decomposition rate constant for the liquid, $m^{1.5} \cdot kg^{-0.5} \cdot s^{-1}$

L – column height, m

M – molecular weight, $kg \cdot mol^{-1}$

m – Henry's law constant (dimensionless), –

N – mass transfer flux, $m^3 \cdot kg^{-1} \cdot s^{-1}$

Pe – Peclet number, –

P – pressure, Pa

P_0 – atmospheric pressure, Pa

P_t – total pressure, Pa

R – gas constant, $Pa \cdot m^3 \cdot mol^{-1} \cdot K^{-1}$

T – absolute temperature, K

t_p – average residence time, s

U – superficial gas velocity, $m \cdot s^{-1}$

X – dissolved organic substance concentration, $kg \cdot m^{-3}$

z – axial height, m

ε_G – gas holdup, –

μ – viscosity, $Pa \cdot s$

ρ – density, $kg \cdot m^{-3}$

σ – surface tension, $kg \cdot s^{-2}$

σ_p – standard deviation of R.T.D., s

τ_w – wall shear rate, $kg \cdot m^{-1} \cdot s^{-2}$

Subscripts

e – exit

G – gas

i – *i*-th tank

int – inner tube

j – gaseous species

L – liquid

O – odorous material

out – outer column

S – ozone consuming substances

0 – inlet, standard condition

References

1. *Somiya, I.*, Water treatment using ozone (in Japanese), Kogai Taisaku Gijutu Doyukai (1989).

2. *Sato, A.*, Water treatment-its new development (in Japanese). Gihoudou Shuppan (1992).

3. *Roustan, M., Line, A., Brodard, E., Duguet, J. P., Mallevialle, J.*, Water Supply, **8** (3-4, Water Nagoya '89) (1990) 458-464.

4. *Roustan, M., Line, A., Duguet, J. P., Mallevialle, J., Wable*, O., Ozone Sci. & Eng., **14** (1992) 427-438.

5. *Roustan, M., Line, A., Wable, O.*, Chem. Eng. Sci., **47**(13/14) (1992b) 3681-3688.

6. *Roustan, M., Beck, C., Walbe, O., Duguet, J. P., Mallevialle, J.*, Ozone Sci. & Eng., **15** (1993) 213-226.

7. *Muroyama, K., Norieda, T., Morioka, A., Tsuji, T.*, Chem. Eng. Sci., **54** (1999) 5285-5292.

8. *Muroyama, K., Shimizu, M., Shibutani, E., Tsuji, T.*, Chem. Eng. Sci., **60** (2005) 6350-6370.

9. *Clark, N. N., Flemmer, R.L.*, AIChE J., **31** (1985) 500-503.

10. *Zuber, N., Findlay, J. A.*, Journal of Heat Transfer, **87**(4), (1965) 453-468.

11. Society of Chemical Engineers Japan eds., Kagaku-Kogaku Benran, 6th ed. (in Japanese) Maruzen Book Co. Ltd., 1999.

12. *Miyahara, T., Hirokawa, M., Ueda, M., Yoshida, H.*, Kagaku Kogaku Ronbunshu, **20** (1994) 497-503.

13. *Wilke, C. R., Chang, P.*, AIChE J., **1**(2), (1955) 262-270.

14. *Akita, K., Yoshida, F.*, Ind. Eng. Chem. Process Des. Dev., **12** (1973) 76-80.

15. *Deckwer, W.-D.*, Bubble Column Reactors, John Wiley and Sons Inc., New York, 1992.

16. *Levenspiel, O., Bischoff, K. B.*, Advan. Chem. Eng., **4**, (1963) 95-198.

17. *Morooka, S., Ikezumi K., Kato, Y.*, Kagaku Kogaku Ronbunshu, **4** (1978) 377-380.

18. *Morioka, M., Hoshikawa, H., Motoyama, N., Okada, M., Moniwa, T.*, Suidou Kyoukai Zasshi, **60**(7) (1991) 7-17.

19. *Moniwa, T., Okada, M., Motoyama, N., Morioka, M., Hohsikawa, H.*, Preprint of 42nd meeting of Japan Waterworks Association, **4**(18), (1991) 145-147.

20. *Morioka, T., Motoyama, N., Hoshikawa, H., Murakami, A., Okada, M., Moniwa, T.*, Ozone Sci. & Eng., **15** (1993) 1-18.